

# Enhancement of photon blockade via topological edge states

Jun Li,<sup>1,2,\*</sup> C.-M. Hu,<sup>2,†</sup> and Yaping Yang<sup>1,‡</sup>

<sup>1</sup>*MOE Key Laboratory of Advanced Micro-Structured Materials,*

*School of Physics Science and Engineering, Tongji University, Shanghai, 200092, China*

<sup>2</sup>*Department of Physics and Astronomy, University of Manitoba, Winnipeg R3T 2N2, Canada*

(Dated: November 21, 2023)

Quantum technologies, holding the promise of exponentially superior performance than their classical counterparts for certain tasks, have consistently encountered challenges, including instability in quantum light sources, quantum decoherence and vulnerability to losses that topological photonics happens to adeptly address. Here, we theoretically put forth a quantum Su-Schrieffer-Heeger-type chain designed to greatly enhance single-photon blockade (single-PB) effect with topological protection. By designing the deliberate coupling strengths, the quantum-level lattices take the form of a one-dimensional array with a topological edge state in single-excitation space and a two-dimensional square breathing lattice with topological corner states in two-excitation space, resulting in enhanced single-photon excitation and the suppression of two-photon transitions. Therefore the second-order correlation function is diminished by up to two orders of magnitude at the cavity resonance frequency, accompanied by stronger brightness. Furthermore, the PB effect is robust to local perturbations in cavity-qubit coupling and qubit frequency, benefitting from topological protection.

## I. INTRODUCTION

Since 2005, topological photonics [1, 2], inspired by topological band theory initially discovered in solid-state electron systems, was first proposed in photonic crystals [3, 4] and so far has been extensively investigated across various platforms, including waveguides [5], cavities [6, 7], metamaterials [8], optomechanics [9], ultracold atoms [10], rf circuits [11, 12] and Fock-state lattices [13, 14]. Further, Optical systems also offer unprecedented opportunities to promote the exploration of novel topological physics and actualize exceptional topological phenomena owing to their remarkable flexibility, diversity and unique effects, e.g., non-Hermitian topology [15], Floquet topological insulators [5, 16], topological photonics in synthetic dimensions [17] and nonlinear topological photonics [18].

In the context of bulk-edge correspondence, topological edge states (TESs) in open boundary conditions are naturally robust against local defects and disorders, attributable to the globally defined topological invariants. This characteristic enables a diverse array of devices and applications for addressing pervasive environmental effects by employing topological photonics, such as wireless power transfer [19, 20], optical beam splitter [21], sensor [22] and nonreciprocity [16] in one dimensions based on Su-Schrieffer-Heeger (SSH) model [23] and topological laser [24, 25], slow light [26, 27], channel-drop filter [28] and four-wave mixing [29] in two dimensions. In particular, quantum light, acting as carriers of quantum information and quantum computing, still encounter challenges related to energy dissipation and decoherence

stemming from external environment and system disorder. The emergence of topological photonic states represents a captivating research avenue to tackle this challenge [30, 31]. In recent years, some pioneering experiments have showcased the robust generation and routing of quantum states in topological photonic integrated platforms [32–35].

Photon blockade (PB) effect serves as a significant technique for generating quantum light sources by effectively suppressing certain photon-number excitations in nonlinear systems. There are two physical mechanisms on which PB relies, i.e., the conventional photon blockade (CPB) [36, 37] and the unconventional photon blockade (UPB) [38–40]. Specifically, The CPB is achieved through eigenenergy-level anharmonicity (ELA) originating from strong nonlinearity. The latter is induced by quantum destructive interference (QDI) between two or more individual quantum transition pathways. Generally, in comparison to CPB, the UPB exhibits a higher degree of anti-bunching, but the brightness is relatively poor. Recently, photon anti-bunching and corresponding mean photon number are both substantially improved by combining the conventional ELA-induced and QDI-induced single-photon blockade (single-PB) in a two-qubit driven cavity quantum electrodynamics (QED) system with dipole-dipole interaction [41]. Interestingly, the UPB is proposed to be enhanced in a chain of coupled resonators with exponentially suppressed nonlinearity requirement [42].

In this work, we propose a one-dimensional (1D) topological multi-qubits-one-cavity chain that can achieve single-PB with much smaller second-order correlation function accompanied by larger cavity mean photon number than Jaynes-Cummings (JC) model (single-qubit-cavity system) under same conditions [36]. The quantum topological chain comprises a linear optical cavity and a trivial dimer qubit lattice, established through the weaker coupling between the cavity and the bound-

\* jli\_phys@tongji.edu.cn

† hu@physics.umanitoba.ca

‡ yang\_yaping@tongji.edu.cn

ary qubit. The quantum-level lattice (QLL) in single-excitation space forms as an SSH chain with odd sites and possesses a zero-energy TES localized at the end of single-photon excited state, thereby enabling a stronger intensity of single-photon excitation. Meanwhile, in two-excitation space, the zero-energy dressed state is localized at the corner of two-qubit excited states with absence of a two-photon excited state distribution. Furthermore, the dressed states with near the zero-energy in the second manifold are the bulk states that hold quite weak distribution of two-photon excited state. So that the single-PB effect is significantly enhanced by the distinct TES distributions in the two manifolds. Moreover, the single-PB effect in the quantum topological lattices also demonstrates robustness against the local disturbances in the cavity-qubit coupling strength and the qubit frequency.

## II. MODEL AND QUANTUM-LEVEL LATTICES

As shown in Fig. 1(a), we consider a 1D quantum topological array composed of a single-mode bosonic cavity and  $N_a$  ( $N_a = 2N$ ,  $N$  is the number of unit cells) identical two-level systems (e.g., two-level qubits) arranged in a dimer chain (or SSH lattice) by coupling to their nearest neighbors with alternative hopping amplitudes  $J_1$  and  $J_2$ . The optical cavity is coupled to one of the outermost qubit with the strength  $g$  and coherently driven by a monochromatic pump field with the Rabi frequency  $\eta$  and angular frequency  $\omega_d$ . Here, all the coupling strengths are much smaller than the transition frequency of qubits  $\omega_a$  and the resonant frequency of cavity  $\omega_c$ . In rotating-wave approximation, the Hamiltonian of the driven multi-qubits-cavity system is  $H = H_a + H_c + H_i + H_d$ , where (setting  $\hbar = 1$ )

$$\begin{aligned}
 H_a &= \Delta_a \sum_{i=1}^{N_a} \sigma_+^i \sigma_-^i + J_1 \sum_{i=1}^{N_a/2} (\sigma_+^i \sigma_-^{i+1} + \text{H.c.}) \\
 &\quad + J_2 \sum_{i=1}^{N_a/2-1} (\sigma_+^{i+1} \sigma_-^{i+2} + \text{H.c.}), \\
 H_c &= \Delta_c a^\dagger a, \quad H_i = g (a^\dagger \sigma_-^1 + \text{H.c.}), \\
 H_d &= \eta (a^\dagger + a),
 \end{aligned} \tag{1}$$

where  $\Delta_a = \omega_a - \omega_d$  is the qubit detuning with respect to the driving frequency and  $\Delta_c = \omega_c - \omega_d$  is the cavity-driving detuning. Here, we focus on the simplest scenario where the frequency of the cavity and the qubits are identical ( $\omega_a = \omega_c = \omega_0$ ), i.e.,  $\Delta_a = \Delta_c = \Delta$ .  $\sigma_+^i = |e\rangle\langle g|_i$  ( $\sigma_-^i = |g\rangle\langle e|_i$ ) is the raising (lowering) operator of the  $i$ th two-level system and  $a^\dagger$  ( $a$ ) is the creation (annihilation) operation of the intracavity optical field.

In single-excitation space, the QLL of the system takes the form of a 1D finite SSH chain with an odd number of sites ( $N_a + 1$ ), which is identical to its classical lattice counterpart [see an example for  $N_a = 4$  shown in Fig.

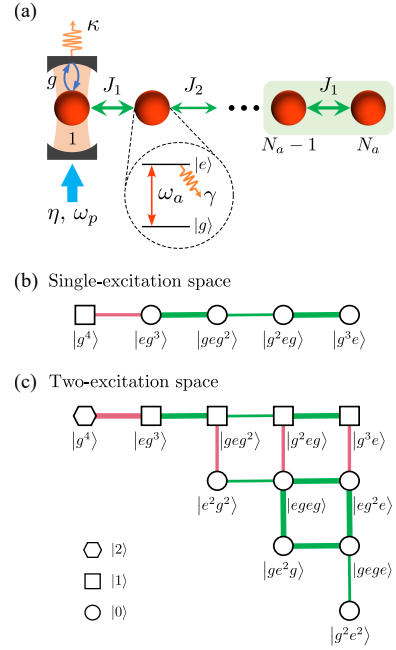


FIG. 1. (a) Schematic of considered multi-qubits-cavity topological chain characterized by an optical cavity (resonant frequency  $\omega_c$ ) coupled to the first site of a dimer two-level lattice with the strength  $g$ . The dimer lattice, whose unit cell are marked by a green box, consists of  $N_a$  identical two-level qubits with the transition frequency  $\omega_a$  between ground state  $|g\rangle$  and excited state  $|e\rangle$ . The intracell and intercell hopping amplitudes of the lattice are  $J_1$  and  $J_2$ , respectively. The cavity (qubit) decay rate is  $\kappa$  ( $\gamma$ ). QLL in (b) single-excitation space and (c) two-excitation space for  $N_a = 4$ . The states labeling the lattice sites are the corresponding positional distributions of the qubit states with the power of the exponent representing the number of repetitions of adjacent qubit states. For clarity, we use circles, squares and hexagon in (b) and (c) to denote the cavity photon states  $|0\rangle$ ,  $|1\rangle$  and  $|2\rangle$ , respectively. The widths of the lines connecting neighboring states represent the coupling strengths between them.

1(b)]. The lattice is expanded to two dimensions and comprises  $N_a(N_a + 1)/2 + 1$  sites in two-excitation space for  $N_a \geq 4$ . The quantum states form a square breathing lattice with triangle boundaries, constituting a two-order topological structure as illustrated in Fig. 1(c). In particular, due to the inherent nature of the annihilation operator  $a|n\rangle = \sqrt{n}|n-1\rangle$ , the coupling strength between the two-photon state  $|g^{N_a}, 2\rangle$  and its nearest neighbor state  $|g^{N_a-1}, 1\rangle$  is  $\sqrt{2}g$ . Additionally, the QLL in three-excitation space is represented as a three-dimensional cubic lattice with a triangular pyramid as the outline.

In this study, we consider the condition where  $g < J_1$  and  $J_2 < J_1$  to ensure that the single-photon excited state  $|g^{N_a}, 1\rangle$  is the sole weaker coupling termination in single-excitation lattice. Therefore, it can be inferred that there is an exactly zero-energy state exponentially localized to the end with one-photon excited state. Furthermore, we add the constraint  $J_1 \leq \sqrt{2}g$  in order to

prevent the two-photon state  $|g^{N_a}, 2\rangle$  from being a relatively weaker coupling corner in two-excitation lattice for  $N_a \geq 4$ . Instead the two-qubit excited state  $|g^{N_a-2}e^2, 0\rangle$  always serves as a weakly coupled corner. Thus, the topological zero-energy state in two-excitation space is predominantly distributed at the two-qubit excited states rather than the two-photon excited state. By combining the aforementioned two conditions, it is expected that single-PB effect will occur at the resonance frequency of the cavity.

Based on the Born-Markov approximation, the dynamic density matrix  $\rho$  of the entire system with dissipation is governed by the master equation

$$\frac{\partial \rho}{\partial t} = -i[H, \rho] + \frac{\kappa}{2}\mathcal{L}_\rho[a] + \frac{\gamma}{2}\sum_{i=1}^{N_a}\mathcal{L}_\rho[\sigma_-^i], \quad (2)$$

where  $\mathcal{L}_\rho[a] = 2a\rho a^\dagger - a^\dagger a\rho - \rho a^\dagger a$  indicates the cavity leakage at rate  $\kappa$  and  $\mathcal{L}_\rho[\sigma_-^i] = 2\sigma_-^i\rho\sigma_+^i - \sigma_+^i\sigma_-^i\rho - \rho\sigma_+^i\sigma_-^i$  denotes the spontaneous decay of the excited state of  $i$ th qubit at rate  $\gamma$ .

### III. ENHANCEMENT OF PHOTON BLOCKADE

In the absence of the driven field and system dissipation, we can numerically obtain the eigenvalues  $E_{\pm i}^n$  and their corresponding eigenstates  $\Phi_{\pm i}^n$ , where the superscript  $n \in [0, 1, 2, \dots]$  indicates the order of the manifold and the subscript  $\pm i$  denotes  $i$ th symmetric eigenstates with reference to zero-energy in each space. By setting the normalized hopping amplitudes  $J_1/g = \sqrt{2}$  and  $J_2/g = 0.2$ , we plot the corresponding eigenvalue structures of our topological array for the simpler cases of  $N_a = 2$  in Fig 2(b) and  $N_a = 4$  in Fig 2(c), respectively. As expected, in the first manifold, there always exists an exact zero-energy dressed state  $\Phi_0^1 = C_1|g^{N_a}, 1\rangle + C_2|eg^{N_a-1}, 0\rangle + \dots + C_{N_a+1}|g^{N_a-1}e, 0\rangle$  that is exponentially localized at the single-photon excited state  $|g^{N_a}, 1\rangle$  (as exemplified in Fig. 2(d) for  $N_a = 4$ ), with the normalized amplitudes  $C_1 > 0.8$  and  $C_{2x} = 0$  ( $x \in [1, \dots, N]$ ) as  $N_a$  varies. In the second manifold, the zero-energy dressed level is absent for the simplest case of  $N_a = 2$  as shown in Fig 2(b). For  $N_a \geq 4$ , there are  $N_a/2 - 1$  zero-energy states primarily distributed among the two-qubit excited states, without any distribution at the two-photon excited state (as shown in Fig. 2(f) for  $N_a = 4$ ). Moreover, for comparison, we include the dressed state diagram of coupled single-qubit-cavity system (JC model) in Fig 2(a), where there is no zero-energy state in any manifold.

The single-PB effect behaviors are quantified by the equal-time second-order correlation function  $g^{(2)}(0)$ , which can be calculated by

$$g^{(2)}(0) = \frac{\langle a^{\dagger 2} a^2 \rangle}{\langle a^\dagger a \rangle^2} = \frac{\text{Tr}(a^{\dagger 2} a^2 \rho)}{[\text{Tr}(a^\dagger a)]^2}, \quad (3)$$

where the density matrix  $\rho$  is obtained by numerically solving Eq. (2) based on the QuTiP [43] and the QuantumOptics.jl toolbox [44].

With the same normalized system parameters  $g/\gamma = 10$  and  $\kappa/\gamma = 0.5$ , figures 3(a-c) show the logarithmic plots of equal-time second-order correlation function  $\log_{10}[g^{(2)}(0)]$  as a function of the detuning  $\Delta/\gamma$  and driven strength  $\eta/\gamma$  for different numbers of qubits  $N_a = 1, 2$  and 4, respectively. The corresponding mean photon number  $\langle a^\dagger a \rangle$  are displayed in Figs. 3(d-f). In the single-qubit case, single-PB occurs around the detuning  $\Delta = \pm g$  due to the single-photon resonance with non-resonant two-photon excitations as depicted in Fig. 2(a) [36, 37]. For our multi-qubits-cavity topological chain, as clearly shown in Figs. 3(b) and 3(c), there are three regimes of single-PB ( $g^{(2)}(0) < 1$ ) with the detuning  $\Delta = 0$  and  $\Delta \approx \pm 1.8g$  on the plane, which correspond to the single-photon excitation process from the ground state  $|g^{N_a}, 0\rangle$  to the TES  $\Phi_0^1$  and the bulk states  $\Phi_{\pm N_a/2}^1$  of QLL in single-excitation space respectively. Particularly, the resonance-driven scenario shows a significantly smaller second-order correlation function, indicating strong single-photon antibunching. Meanwhile, higher mean photon number peak concomitantly appears due to the stronger single-photon excitation probability. Moreover, the frequency range for achieving single-PB around  $\Delta = 0$  slightly expands as the number of qubits  $N_a$  increases.

For the sake of comparison, we present the optimal second-order correlation function  $\log_{10}[g^{(2)}(0)]$  in the frequency domain against the normalized pump strength  $\eta/\gamma$  for different numbers of qubits in Fig. 3(g), along with the corresponding mean photon number  $\langle a^\dagger a \rangle$  in Fig. 3(h). Obviously, in comparison to the JC model ( $N_a = 1$ ), the multi-qubits-cavity lattices ( $N_a \geq 2$ ) exhibit up to two orders of magnitude smaller  $g^{(2)}(0)$ , accompanied by larger mean photon number. For two-qubits case, the enhancement of single-PB arises from the greater two-photon excitation anharmonicity and the lower two-photon intensity of dressed states in the second manifold in contrast to the JC model. With an increasing number of qubits ( $N_a \geq 4$ ), as depicted in Fig. 2(c), the number of dressed levels in the second manifold increases quadratically, resulting in smaller anharmonicity and the emergence of zero-energy dressed states  $\Phi_0^2$ . However, in the resonance-driven case, there is only a slight variation in the second-order correlation function and the mean photon number. On the one hand, the resonant transition  $\Phi_0^1 \rightarrow \Phi_0^2$  is strictly forbidden due to the lack of overlap between the wavefunction distributions of the zero-energy states in the two manifolds on the same qubit states, as shown in Figs 2(d) and 2(f). On the other hand, the dressed states with near-zero energy in the second manifold correspond to bulk states characterized by a weak intensity of two-photon state  $|g^{N_a}, 2\rangle$  [see Figs. 2(e) and 2(g)]. Further, the intensity decreases as the number of qubits  $N_a$  increases, leading to the expansion of single-PB region around  $\Delta = 0$ .

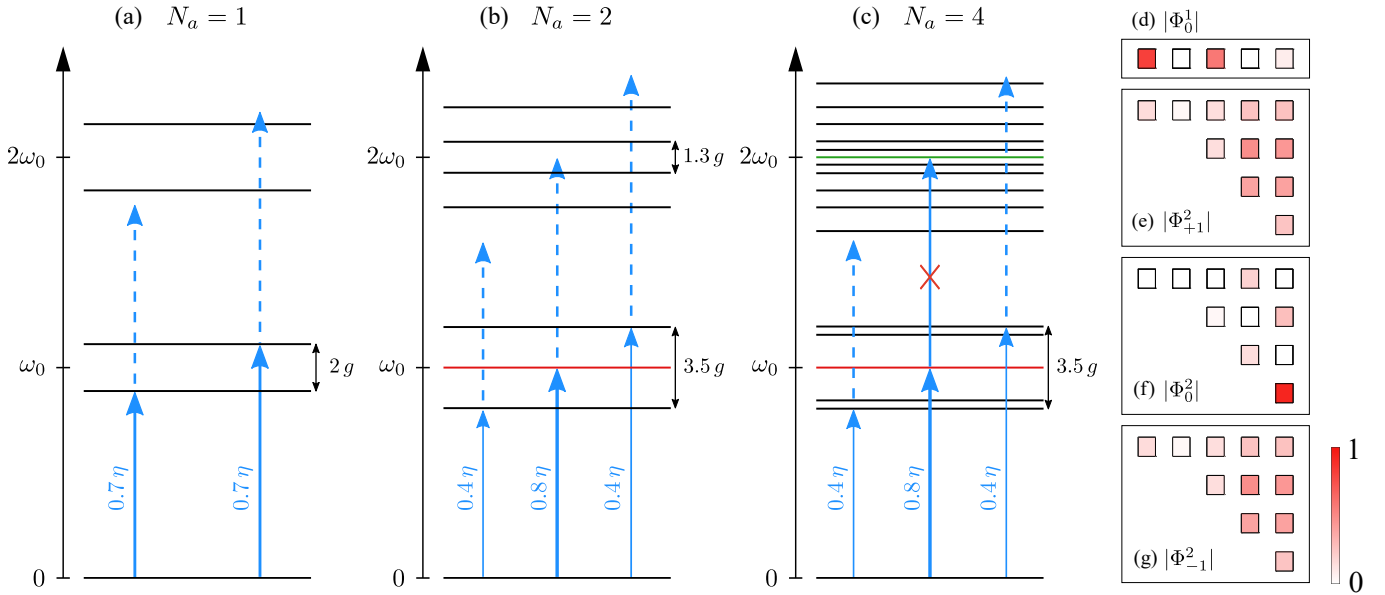


FIG. 2. The dressed state structures and the main transition pathways of considered qubit-cavity coupled system with the number of qubits (a)  $N_a = 1$  (JC model), (b)  $N_a = 2$  and (c)  $N_a = 4$ . The levels labeled by red in (b) and (c) are the topological edge modes in single-excitation space while the green level in (c) is the topological corner state in two-excitation space. The single blue arrows in (a-c) denote the excitation pathways of photon blockade (PB) where the dashed arrows indicate the ELA. The wavefunction distributions of (d) the topological zero-energy states  $|\Phi_0^1\rangle$  in single-excitation space, (e, g) the zero-energy corner-localized state  $\Phi_0^2$  and (e, g) the bulk states  $\Phi_{\pm 1}^2$  in two-excitation space for  $N_a = 4$ . The layout of sites in (d) and (e-g) is accordance with that shown in Fig. 1(b) and 1(c), respectively. Here, we take the parameter relations  $J_1 = \sqrt{2}g$  and  $J_2 = 0.2g$ .

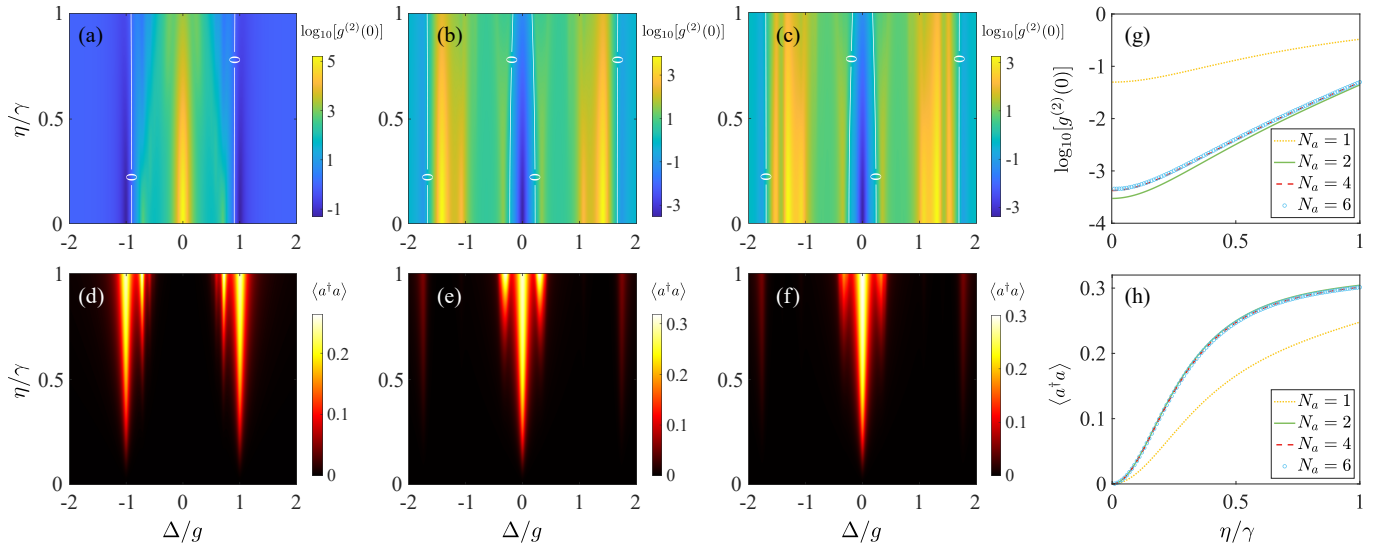


FIG. 3. (a-c) The equal-time second-order correlation function  $\log_{10}[g^{(2)}(0)]$  and (d-f) the corresponding mean photon number  $\langle a^\dagger a \rangle$  mapping on the plane of normalized detuning  $\Delta/g$  and driven strength  $\eta/\gamma$  for (a, d)  $N_a = 1$ , (b, e)  $N_a = 2$  and (c, f)  $N_a = 4$ , respectively. The white curves in (a-c) denote the contours of  $g^{(2)}(0) = 1$  for Poissonian statistics. (g) The optimal second-order correlation function and (h) the corresponding mean photon number versus the normalized pump field Rabi frequency  $\eta/\gamma$  for different  $N_a$ . The optimal condition are  $\Delta/g = \pm 1$  for  $N_a = 1$  and  $\Delta = 0$  for  $N_a \geq 2$ . Here, the system parameters are given by  $g = 10\gamma$  and  $\kappa = 0.5\gamma$ . The other parameters are the same as those used in Fig. 2.



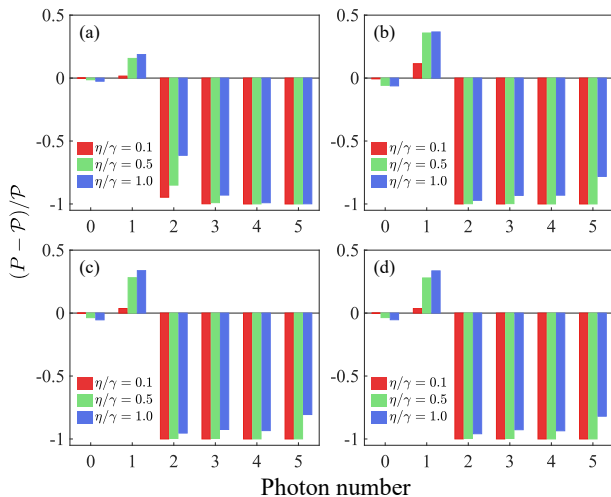


FIG. 4. The deviations of the photon distribution to the standard Poisson distribution with the same mean photon number for (a)  $N_a = 1$ , (b)  $N_a = 2$ , (c)  $N_a = 4$  and (d)  $N_a = 6$ , respectively. The cavity-driving detuning is  $\Delta = \pm g$  for  $N_a = 1$  and  $\Delta = 0$  for  $N_a \geq 2$ . The other system parameters are the same as those used in Fig. 3.

The enhancement of single-PB can be further confirmed by comparing the photon-number distribution of the cavity field  $P(n)$  with the Poisson distribution  $\mathcal{P}(n) = \langle a^\dagger a \rangle^n e^{-\langle a^\dagger a \rangle} / n!$ . In Fig. 4, we show the relative deviations of photon number distribution with respect to the Poisson distribution with the same mean photon number, i.e.,  $[P(n) - \mathcal{P}(n)] / \mathcal{P}(n)$ . In comparison to the JC model ( $N_a = 1$ ) with the identical conditions, it is evident that  $P(1)$  in the multi-qubits-cavity system ( $N_a \geq 2$ ) is more strongly enhanced while  $P(n > 1)$  are significantly suppressed, indicating the higher probability for detecting a single photon. Moreover, the probability distribution  $P(1)$  is also greatly enhanced as the driven strength increases.

#### IV. ROBUSTNESS OF PHOTON BLOCKADE

The PB effect of our quantum topological array effectively incorporates and demonstrates the inherent topological protection property of the SSH chain that are insensitive to local perturbations. Here, we examine the robustness of the single-PB phenomenon in the presence of perturbations by considering specific examples of disturbances in the cavity-qubit coupling strength  $\delta_g$  and the transition frequency of the first qubit  $\delta_{\omega 1}$ . In Fig. 5, by considering the cavity-qubit coupling strength  $g' = g + \delta_g$ , we present the evolution of the second-order correlation function  $\log_{10}[g^{(2)}(0)]$  and the corresponding cavity mean photon number  $\langle a^\dagger a \rangle$  versus the fluctuation strength of cavity-qubit coupling  $\delta_g$  with  $\eta/\gamma = 0.5$  for different  $N_a$ . Predictably, in the JC model, the optimal operating frequency for achieving single-PB experiences a linear shift

in response to the fluctuation strength of the cavity-qubit coupling due to the linear coupling-dependent dressed levels in the first manifold. In contrast, in the case of multi-qubits-cavity arrays ( $N_a \geq 2$ ), the optimal operating frequency, which yields the smallest second-order correlation function  $g^{(2)}(0)$  and the largest mean photon number  $\langle a^\dagger a \rangle$ , consistently remains at the resonance frequency of the cavity regardless of variations in the cavity-qubit coupling strength. For the resonance-driven condition,  $g^{(2)}(0)$  and the mean photon number  $\langle a^\dagger a \rangle$  decrease (increase) with increasing (decreasing) cavity-qubit coupling strength, owing to the heightened (depressed) two-photon excitation anharmonicity and single-photon excitation probability, respectively. As clearly shown in Figs. 5(g) and 5(h), compared with the single-qubit cavity system, the second-order correlation function and mean photon number of the quantum topological arrays are more robust to the cavity-qubit coupling fluctuation at a fixed operating frequency.

For the diagonal perturbation, we show the developments of correlation function and corresponding cavity mean photon number with the normalized frequency shift of the qubit coupled to cavity  $\delta_{\omega 1}/\gamma$  as shown in Fig. 5. For single qubit condition, the optimal pump frequency to achieve PB with a brighter mean photon number is directly related to the qubit frequency, which is not conducive to manipulation in practical applications. Contrastingly, the multi-qubits-cavity chain maintains an almost constant mean photon number at the cavity resonance frequency, given that the frequency and distribution of TES in the single-excitation space are hardly affected by the transition frequency of the qubit. Simultaneously, in the two-excitation space, the distribution density of the zero-energy state on the two-photon excited state is no longer entirely zero with a nonzero qubit frequency shift. This leads to a gradual increase in the second-order correlation function with the increasing qubit frequency shift for the resonance-driven condition.

#### V. CONCLUSION

In summary, we have investigated an enhanced conventional photon blockade effect utilizing a 1D cascading coupled multi-qubits-one-cavity array based on the SSH model. One-sided localized topological edge states of the QLL in single-excitation space empower the system to exhibit a stronger intensity of single-photon excitation at the resonance frequency while two-photon excitation is effectively suppressed due to the forbidden resonance excitation and diffusely distributed bulk states in two-excitation space. The quantum topological chain exhibits a robust single-PB effect, achieving up to a two-order magnitude improvement in the second-order correlation function yet enhancing the mean photon number simultaneously. Our work contributes a theoretical framework for the preparation of stable quantum light sources leveraging topological states. The implementation of our

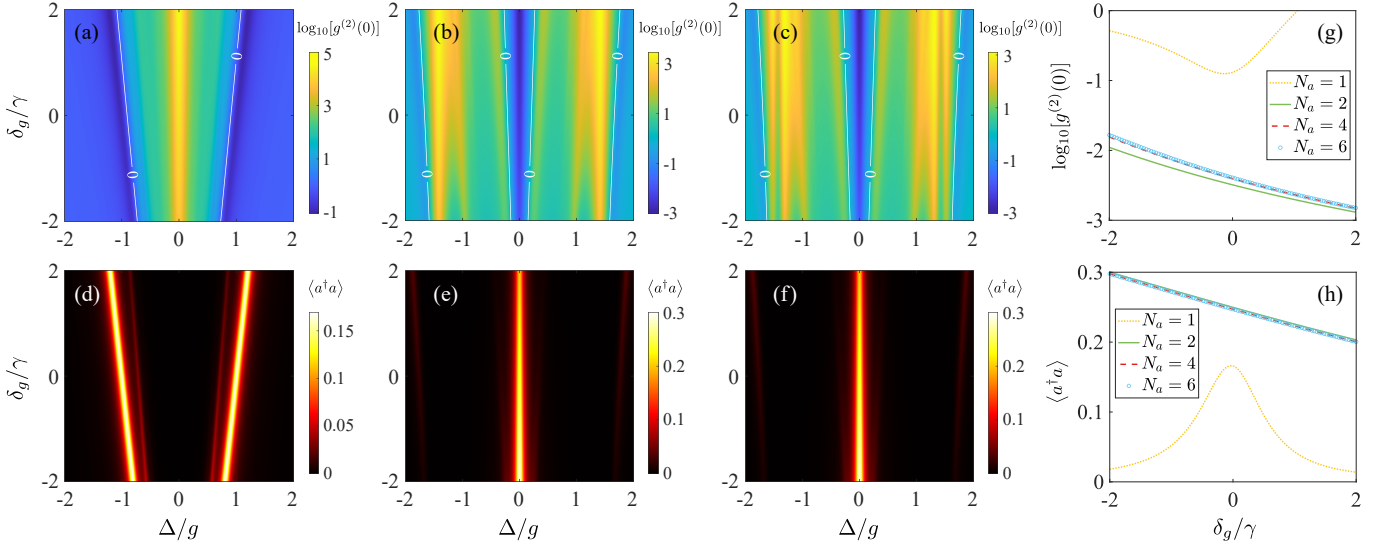


FIG. 5. The influences of fluctuation strength of cavity-qubit coupling  $\delta_g$ . (a-c) Steady-state second-order correlation function  $\log_{10}[g^{(2)}(0)]$  and (d-f) cavity mean photon number  $\langle a^\dagger a \rangle$  plotted as a function of the normalized detuning  $\Delta/g$  and fluctuation strength  $\delta_g/\gamma$  with the driven strength  $\eta/\gamma = 0.5$  for (a, d)  $N_a = 1$ , (b, e)  $N_a = 2$  and (c, f)  $N_a = 4$ , respectively. (g) The second-order correlations and (h) the corresponding mean photon number in relation to the normalized fluctuation strength  $\delta_g/\gamma$  with the detuning  $\Delta = \pm g$  for  $N_a = 1$  and  $\Delta = 0$  for  $N_a \geq 2$ . All other parameters remain the same as those utilized in Fig. 3.

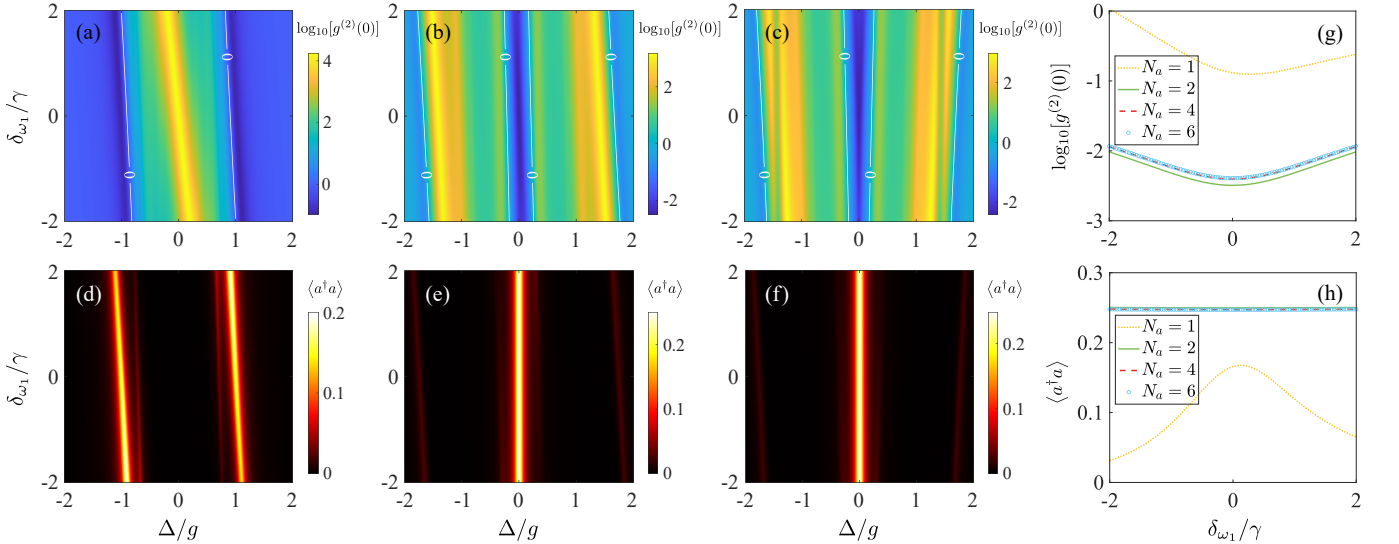


FIG. 6. The effects of first qubit's transition frequency shift  $\delta_{\omega_1}$ . Plots of (a-c)  $\log_{10}[g^{(2)}(0)]$  and (d-f)  $\langle a^\dagger a \rangle$  as a function of the normalized detuning  $\Delta/g$  and frequency shift  $\delta_{\omega_1}/\gamma$  with  $\eta/\gamma = 0.5$  for (a, d)  $N_a = 1$ , (b, e)  $N_a = 2$  and (c, f)  $N_a = 4$ , respectively. Profiles of (g) the second-order correlation function and (h) the corresponding mean photon number at the cavity-driving detuning  $\Delta = g$  for  $N_a = 1$  and  $\Delta = 0$  for  $N_a \geq 2$ . The other system parameters are the same as those employed in Fig. 3.

scheme can potentially be demonstrated in quantum systems such as coupled atom arrays cavity QED [45, 46] and circuit QED system [47, 48].

National Natural Science Foundation of China (12274326); National Key Research and Development

Program of China (2021YFA1400600, 2021YFA1400602); China Scholarship Council (202106260079). C.-M. Hu acknowledges the support from NSERC Discovery Grants and NSERC Discovery

- [1] L. Lu, J. D. Joannopoulos, and M. Soljačić, *Nature Photonics* **8**, 821 (2014).
- [2] T. Ozawa, H. M. Price, A. Amo, N. Goldman, M. Hafezi, L. Lu, M. C. Rechtsman, D. Schuster, J. Simon, O. Zilberberg, and I. Carusotto, *Rev. Mod. Phys.* **91**, 015006 (2019).
- [3] F. D. M. Haldane and S. Raghu, *Phys. Rev. Lett.* **100**, 013904 (2008).
- [4] Z. Wang, Y. Chong, J. D. Joannopoulos, and M. Soljačić, *Nature* **461**, 772 (2009).
- [5] M. C. Rechtsman, J. M. Zeuner, Y. Plotnik, Y. Lumer, D. Podolsky, F. Dreisow, S. Nolte, M. Segev, and A. Szameit, *Nature* **496**, 196 (2013).
- [6] M. Hafezi, E. A. Demler, M. D. Lukin, and J. M. Taylor, *Nature Physics* **7**, 907 (2011).
- [7] K. Fang, Z. Yu, and S. Fan, *Nature Photonics* **6**, 782 (2012).
- [8] S. Ma, B. Yang, and S. Zhang, *Photonics Insights* **1**, R02 (2022).
- [9] M. Schmidt, S. Kessler, V. Peano, O. Painter, and F. Marquardt, *Optica* **2**, 635 (2015).
- [10] N. R. Cooper, J. Dalibard, and I. B. Spielman, *Rev. Mod. Phys.* **91**, 015005 (2019).
- [11] V. V. Albert, L. I. Glazman, and L. Jiang, *Phys. Rev. Lett.* **114**, 173902 (2015).
- [12] J. Ningyuan, C. Owens, A. Sommer, D. Schuster, and J. Simon, *Phys. Rev. X* **5**, 021031 (2015).
- [13] H. Cai and D.-W. Wang, *National Science Review* **8**, 10.1093/nsr/nwaa196 (2020).
- [14] J. Deng, H. Dong, C. Zhang, Y. Wu, J. Yuan, X. Zhu, F. Jin, H. Li, Z. Wang, H. Cai, C. Song, H. Wang, J. Q. You, and D.-W. Wang, *Science* **378**, 966 (2022).
- [15] E. J. Bergholtz, J. C. Budich, and F. K. Kunst, *Rev. Mod. Phys.* **93**, 015005 (2021).
- [16] J. Li, B. Gao, C. Zhu, J. Xu, and Y. Yang, *Applied Physics Letters* **119**, 141108 (2021).
- [17] E. Lustig and M. Segev, *Adv. Opt. Photon.* **13**, 426 (2021).
- [18] D. Smirnova, D. Leykam, Y. Chong, and Y. Kivshar, *Applied Physics Reviews* **7**, 021306 (2020).
- [19] J. Song, F. Yang, Z. Guo, X. Wu, K. Zhu, J. Jiang, Y. Sun, Y. Li, H. Jiang, and H. Chen, *Phys. Rev. Applied* **15**, 014009 (2021).
- [20] L. Zhang, Y. Yang, Z. Jiang, Q. Chen, Q. Yan, Z. Wu, B. Zhang, J. Huangfu, and H. Chen, *Science Bulletin* <https://doi.org/10.1016/j.scib.2021.01.028> (2021).
- [21] W. Song, W. Sun, C. Chen, Q. Song, S. Xiao, S. Zhu, and T. Li, *Laser & Photonics Reviews* **14**, 1900193 (2020).
- [22] Z. Guo, T. Zhang, J. Song, H. Jiang, and H. Chen, *Photon. Res.* **9**, 574 (2021).
- [23] W. P. Su, J. R. Schrieffer, and A. J. Heeger, *Phys. Rev. Lett.* **42**, 1698 (1979).
- [24] G. Harari, M. A. Bandres, Y. Lumer, M. C. Rechtsman, Y. D. Chong, M. Khajavikhan, D. N. Christodoulides, and M. Segev, *Science* **359**, eaar4003 (2018).
- [25] M. A. Bandres, S. Wittek, G. Harari, M. Parto, J. Ren, M. Segev, D. N. Christodoulides, and M. Khajavikhan, *Science* **359**, eaar4005 (2018).
- [26] H. Yoshimi, T. Yamaguchi, Y. Ota, Y. Arakawa, and S. Iwamoto, *Opt. Lett.* **45**, 2648 (2020).
- [27] G. Arregui, J. Gomis-Bresco, C. M. Sotomayor-Torres, and P. D. Garcia, *Phys. Rev. Lett.* **126**, 027403 (2021).
- [28] J.-X. Fu, J. Lian, R.-J. Liu, L. Gan, and Z.-Y. Li, *Applied Physics Letters* **98**, 211104 (2011).
- [29] J. W. You, Z. Lan, and N. C. Panouiu, *Science Advances* **6**, eaaz3910 (2020).
- [30] Q. Yan, X. Hu, Y. Fu, C. Lu, C. Fan, Q. Liu, X. Feng, Q. Sun, and Q. Gong, *Advanced Optical Materials* **9**, 2001739 (2020).
- [31] A. Blanco-Redondo, *Proceedings of the IEEE* **108**, 837 (2020).
- [32] S. Barik, A. Karasahin, C. Flower, T. Cai, H. Miyake, W. DeGottardi, M. Hafezi, and E. Waks, *Science* **359**, 666 (2018).
- [33] A. Blanco-Redondo, B. Bell, D. Oren, B. J. Eggleton, and M. Segev, *Science* **362**, 568 (2018).
- [34] S. Mittal, E. A. Goldschmidt, and M. Hafezi, *Nature* **561**, 502 (2018).
- [35] M. Wang, C. Doyle, B. Bell, M. J. Collins, E. Magi, B. J. Eggleton, M. Segev, and A. Blanco-Redondo, *Nanophotonics* **8**, 1327 (2019).
- [36] K. M. Birnbaum, A. Boca, R. Miller, A. D. Boozer, T. E. Northup, and H. J. Kimble, *Nature* **436**, 87 (2005).
- [37] C. Hamsen, K. N. Tolazzi, T. Wilk, and G. Rempe, *Phys. Rev. Lett.* **118**, 133604 (2017).
- [38] T. C. H. Liew and V. Savona, *Phys. Rev. Lett.* **104**, 183601 (2010).
- [39] H. Flayac and V. Savona, *Phys. Rev. A* **96**, 053810 (2017).
- [40] H. J. Snijders, J. A. Frey, J. Norman, H. Flayac, V. Savona, A. C. Gossard, J. E. Bowers, M. P. van Exter, D. Bouwmeester, and W. Löffler, *Phys. Rev. Lett.* **121**, 043601 (2018).
- [41] C. J. Zhu, K. Hou, Y. P. Yang, and L. Deng, *Photon. Res.* **9**, 1264 (2021).
- [42] Y. Wang, W. Verstraelen, B. Zhang, T. C. H. Liew, and Y. D. Chong, *Phys. Rev. Lett.* **127**, 240402 (2021).
- [43] J. Johansson, P. Nation, and F. Nori, *Computer Physics Communications* **183**, 1760 (2012).
- [44] S. Krämer, D. Plankensteiner, L. Ostermann, and H. Ritsch, *Computer Physics Communications* **227**, 109 (2018).
- [45] A. Cidrim, T. S. do Espirito Santo, J. Schachenmayer, R. Kaiser, and R. Bachelard, *Phys. Rev. Lett.* **125**, 073601 (2020).
- [46] L. A. Williamson, M. O. Borgh, and J. Ruostekoski, *Phys. Rev. Lett.* **125**, 073602 (2020).
- [47] C. Jones, M. A. Fogarty, A. Morello, M. F. Gyure, A. S. Dzurak, and T. D. Ladd, *Phys. Rev. X* **8**, 021058 (2018).
- [48] X. Mi, M. Sonner, M. Y. Niu, K. W. Lee, B. Foxen, R. Acharya, I. Aleiner, T. I. Andersen, F. Arute, K. Arya, A. Asfaw, J. Atalaya, J. C. Bardin, J. Basso, A. Bengtsson, G. Bortoli, A. Bourassa, L. Brill, M. Broughton, B. B. Buckley, D. A. Buell, B. Burkett, N. Bushnell, Z. Chen, B. Chiaro, R. Collins, P. Conner, W. Courtney, A. L. Crook, D. M. Debroy, S. Demura, A. Dunsworth, D. Eppens, C. Erickson, L. Faoro, E. Farhi, R. Fatemi, L. Flores, E. Forati, A. G. Fowler, W. Giang, C. Gidney, D. Gilboa, M. Giustina, A. G. Dau, J. A. Gross, S. Habegger, M. P. Harrigan, M. Hoffmann, S. Hong, T. Huang, A. Huff, W. J. Huggins, L. B. Ioffe, S. V. Isakov, J. Iveland, E. Jeffrey, Z. Jiang, C. Jones, D. Kafri,

K. Kechedzhi, T. Khattar, S. Kim, A. Y. Kitaev, P. V. Klimov, A. R. Klots, A. N. Korotkov, F. Kostritsa, J. M. Kreikebaum, D. Landhuis, P. Laptev, K.-M. Lau, J. Lee, L. Laws, W. Liu, A. Locharla, O. Martin, J. R. McClean, M. McEwen, B. M. Costa, K. C. Miao, M. Mohseni, S. Montazeri, A. Morvan, E. Mount, W. Mruczkiewicz, O. Naaman, M. Neeley, C. Neill, M. Newman, T. E. O'Brien, A. Opremcak, A. Petukhov, R. Potter, C. Quin-

tana, N. C. Rubin, N. Saei, D. Sank, K. Sankaragomathi, K. J. Satzinger, C. Schuster, M. J. Shearn, V. Shvarts, D. Strain, Y. Su, M. Szalay, G. Vidal, B. Villalonga, C. Vollgraff-Heidweiller, T. White, Z. Yao, P. Yeh, J. Yoo, A. Zalcman, Y. Zhang, N. Zhu, H. Neven, D. Bacon, J. Hilton, E. Lucero, R. Babbush, S. Boixo, A. Megrant, Y. Chen, J. Kelly, V. Smelyanskiy, D. A. Abanin, and P. Roushan, *Science* **378**, 785 (2022).